Macromolecules

pubs.acs.org/Macromolecules Article

Crystallization of Long-Spaced Precision Polyacetals II: Effect of Polymorphism on Isothermal Crystallization Kinetics

Xiaoshi Zhang, Stephanie F. Marxsen, Patrick Ortmann, Stefan Mecking, and Rufina G. Alamo*

Cite This: *Macromolecules* 2020, 53, 7899−7913 Read Online

ACCESS | Metrics & More | Article Recommendations | Supporting Information

ABSTRACT: Under isothermal crystallization (T_c) from the melt, polyacetals spaced by 12, 18, 19, or 23 methylenes develop two or three distinctive layered polymorphs. The polymorphs formed in the lowest T_c range are kinetically favored (hexagonal and Form I) and characterized by highly nucleated small axialites up to T_c very close to their melting point. In the higher range of T_c, a thermodynamically more stable Form II develops that melts at 5−8 degrees higher temperatures and forms large spherulites. Form I and Form II overlap in a very small range of T_c. While the overall crystallization kinetics of Form I display the usual negative temperature coefficient, an inversion of the dependence of the rate of Form II with temperature occurs when approaching from above the narrow T_c range where Form I and Form II coexist. The inversion is attributed to a competition in nucleation between Form I and Form II. Just before inception of Form II, the crystallization rate is so low that it becomes basically extinguished. The degree of crystallinity recovers when pure Form II develops with a small increase in T_c. Although in the overlapping range, the growth rates of Form I are significantly lower than those of Form II, compared at a fixed undercooling, the rates of Form I are one order of magnitude higher than those of Form II. The difference is attributed to a two to six times higher energy barrier for nucleation of Form II, calculated from analysis of growth rate data according to surface nucleation theory. Such a difference explains the observed variation in nucleation density between the two polymorphs. A minimum in the growth rate of Form I of PA-12, consistent with the effect of "self-poisoning", occurs at T_c approaching the melting point of the hexagonal phase from above.

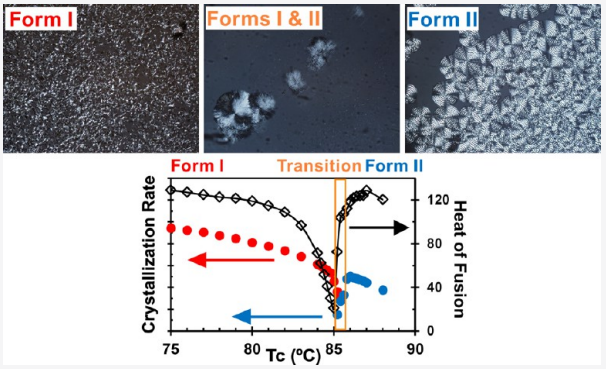

INTRODUCTION

In a preceding work, we demonstrated that rapidly crystallized long-spaced polyacetals undergo melting-recrystallization-melting events on heating.[1] The recrystallization events demarcate reorganization into a more stable layered crystalline polymorph that, upon further heating, melts at a higher temperature. Under fast crystallization from the melt to 20 °C, the polyacetals develop a disordered structure (odd-spaced) or a mixture of disordered and Form I crystals (even-spaced). On heating from 20 to 50−70 °C, the disordered structure reorganizes to hexagonal-like crystals, which further melt and recrystallize into Form I crystallites. A drastic change in the X-ray diffractogram, from a broad single-peak pattern to multiple sharp reflections indicative of crystallographic planes of a different crystal structure, characterizes the polymorphic transitions. On continuous heating, Form I crystals melt and quickly recrystallize into a fourth polymorph, Form II, which further melts at about 10 °C higher temperatures.[1]

Melting-recrystallization-melting events are commonly found in the melting thermograms of precision polyethylene-like systems, often indicating the transformation, on heating, from one crystal form to another with higher thermal stability.[2−15] Moreover, upon analysis of isothermal crystallization rates over a wide range of temperatures covering polymorphic transitions in other semicrystalline polymers, minima or discontinuities in the negative coefficient of the crystallization rates are often observed at temperatures within the transition between polymorphs.[16−25] Rate discontinuities found in PLA and other polyesters are explained as a competition between primary nucleation and radial growth of the two crystal modifications.[16,19,20] Similarly, fast scanning calorimetric measurements of the overall crystallization rates of different polyamides display two maxima with increasing temperature overlapping at the intersection between two polymorphic forms. Coupled with morphological studies, the maxima were interpreted as a combined change in crystal structure and nucleation mechanisms.[26−28] Recently, a deep minimum in the variation of the growth rate with temperature

Received: June 19, 2020
Revised: August 3, 2020
Published: August 31, 2020

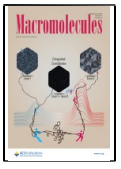

https://dx.doi.org/10.1021/acs.macromol.0c01443
Macromolecules 2020, 53, 7899−7913

was found in precision polyethylenes with halogens.[2] For example, in a series of bromine-containing precision polyethylenes spaced between 9 and 21 carbons, a sharp transition from an *all-trans* planar (Form I) structure to a nonplanar herringbone (Form II) structure takes place on heating crystals of the first type. Both forms are found to coexist in a narrow range of crystallization temperatures (within 2−3 degrees). At temperatures below this range, the kinetically favored Form I crystals develop. Form II crystals are more stable as they are formed and melt at higher temperatures.

Of particular interest is the crystallization kinetics in the temperature range demarcated by the melting points of both polymorphs, i.e., the unusual growth rate kinetics of the most stable phase (Form II). Indeed, the temperature coefficient of the nucleation and growth rates of Form II displays a discrete minimum with decreasing crystallization temperature near (but above) the melting point of Form I.[2] Interpreted as a "self-poisoning" effect, previously studied long-chain *n*-alkanes with >150 backbone carbons also show this unusual feature.[29−32] At high temperatures, long-chain *n*-alkanes form extended-chain crystals and form integer folded-chain crystals at lower temperatures. At crystallization temperatures approaching the melting point of once folded crystals from above, deposition of once folded segments on the surface of extended crystallites temporarily retards growth until the once folded segments detach, thus causing a decrease in the growth rate. The growth rate increases again at lower temperatures in the region of stability of the once folded structure.[33] Following similar arguments, the observed minimum in the growth rate of high-molecular-weight precision polyethylenes with bromine was associated with self-poisoning at the growth front of the herringbone-like Form II crystals by deposition of segments of planar Form I. As growth of Form I cannot proceed at temperatures above their melting point, the segments with the wrong conformation need to detach or reorganize into the structure of Form II for continuation of constructive growth. Consequently, the depth of the observed minimum depends on the relative rates of segmental attachment of Form I and growth of Form II, which depend on the relative rates of nucleation and growth of both forms.[2] The minimum observed in the temperature gradient of the growth rates of precision Br-containing polyethylenes not only corroborated the findings in *n*-alkanes about 30 years earlier but also provided evidence that supports molecular events at the growth front as a major component in the mechanism of growth, via surface nucleation, of high-molecular-weight polymer lamellar crystals.

The series of long-spaced polyacetals also develop different crystal structures within a small change in undercooling. As shown in our previous paper, on slow heating, the kinetically favored Form I melts and quickly recrystallizes into a thermodynamically more stable structure (Form II), which further melts at a higher temperature.[1] The analogy with the melting behavior of precision polyethylenes with bromines makes the series of long-spaced polyacetals good candidates to test the generality of the concept of self-poisoning, especially considering that long-spaced polyacetals develop layered polymorphic crystalline structures controlled by a difference in crystallization kinetics.[1] In the present work, we first identify the range of isothermal crystallization temperatures where Form I and Form II are enabled for polyacetals spaced by an even (12, 18) or odd (19, 23) number of methylenes and further continue with analysis of the overall isothermal crystallization rates and the linear growth rates of these systems with focus in the range of temperatures of the transition between Form I and Form II.

EXPERIMENTAL PART

Materials. Previous works reported the synthesis and molecular weight characterization by GPC or end-group analysis of the long-spaced polyacetals examined here.[34,35] These characterization data, along with the crystallization temperature and the highest melting temperature obtained by DSC at a rate of 10 °C/min, are listed in Table 1. The nomenclature (PA-X) indicates the type of polymer and the number of methylene sequences between two consecutive acetal groups (X = 12, 18, 19, or 23). The repeating structural unit is $-[O-CH_2-O-(CH_2)_x]_n-$.

Table 1. Molecular Mass and Thermal Characterization of Precision Long-Spaced Polyacetals

sample	mol % acetal groups	M_n (kg/mol)	M_w/M_n	$T_{c\ peak}$ (°C)[c]	$T_{m\ peak}$ (°C)[c]
PA-12	8.33	30.2[a]	2.3[a]	48	68.5
PA-18	5.56	16.0[b]		69.5	82.2
PA-19	5.26	13.9[b]		70.5	82.7
PA-23	4.35	8.9[b]		77.3	90.3

[a]Determined by GPC at 160 °C in 1,2,4-trichlorobenzene versus polyethylene standards. [b]Determined by end-group analysis from ^{1}H NMR spectroscopy. [c]Crystallization and highest melting peaks from DSC of samples crystallized and melted at 10 °C/min (data from ref 1).

The initial powders were melted within thin Teflon sheets and cooled down to room temperature to form ∼100 μm films. Pieces of these films were encapsulated in aluminum DSC pans for studies of the overall isothermal crystallization rates. A different piece of the same film was sandwiched between two microscope glass-cover slips for measurements of the isothermal linear growth rates.

Measurements. The overall crystallization rates were measured by differential scanning calorimetry (DSC) or by a combination of DSC and FTIR measurements. For the DSC measurements, the samples were first heated to 150 °C for 5 min and further cooled at a rate of 40 °C/min to the crystallization temperature (T_c). The samples were held at T_c for sufficient time to record the exothermic heat flow. The crystallization rate at any specific T_c was associated with the inverse of the time required to obtain half of the transformation ($1/t_{0.5}$). For symmetric exotherms, $t_{0.5}$ corresponds to the time at the peak of the exotherm.

In the T_c range of coexistence of Form I and Form II, the overall crystallization rate becomes very slow; consequently, the DSC exotherms are shallow and too broad to be sufficiently resolved for kinetic data. For these temperatures, the crystallization rates were obtained from the sigmoidal evolution of the heat of fusion of crystals that develop with increasing crystallization time at T_c. The sigmoidal evolution was constructed by stopping the crystallization after a preset crystallization time. The melting process was recorded from T_c. As Form I and Form II melt at different temperatures, the evolution of each melting peak with time was analyzed to extract independent crystallization kinetics for each form. All thermal data were recorded using a DSC TA2000 under dry N_2 flow. The static temperature, thermal lags, and heat of fusion were calibrated with indium. The TA instrument is connected to an intracooler to maximize heat transfer and allow subambient temperature control. Once the required crystallization time had elapsed, the isothermally crystallized samples were melted at a heating rate sufficiently high to avoid melt-recrystallization. As shown in our prior work, the heating rates needed to avoid recrystallization range from 10 to 80 °C/min depending on the length of the methylene spacer.[1]

Real-time FTIR spectra were collected during isothermal crystallization at the highest and lowest temperatures to extend the T_c range to values impractical for DSC measurements. At the lowest

https://dx.doi.org/10.1021/acs.macromol.0c01443
Macromolecules 2020, 53, 7899−7913

T_c, the DSC cannot bypass crystallization prior to reaching T_c, while the use of a Linkam hot stage and liquid nitrogen cooling accessory allows much faster, controlled cooling rates. FTIR was also used to collect kinetic data at the highest T_c for PA-12 for which the crystallization times are very long. In the latter cases, the increase in the crystalline absorbance at 850 cm^{-1} (CH_2 rocking progression mode) with time was measured as crystallization progresses. The spectra were collected using a Thermo Scientific Nicolet 6700 spectrometer equipped with a TE cooled DTGS TEC detector. Instrumental control and peak analysis were carried out using OMNIC software provided with the instrument. The spectra were collected on absorption mode in a wavenumber range between 4000 and 400 cm^{-1} at a resolution of 2 cm^{-1}. Thin films (~100 μm) were melted between two ~0.2 mm-thick KBr pellets. The KBr sandwich was placed on a Linkam FTIR 600 stage with a TMS94 temperature controller and coupled to a cryogenic cooling unit, all made by Linkam Scientific Instruments Ltd., U.K. The temperature was raised to about 30 °C above the observed melting point and held for 5 min to erase the previous thermal history. The sample was then cooled down to the crystallization temperature at a rate of 100 °C/min to avoid crystallization prior to reaching a low T_c.

Wide-angle X-ray diffraction (WAXD) and small-angle X-ray scattering (SAXS) patterns of isothermally crystallized PA-18, PA-19, and PA-23 were collected simultaneously at the T_c using synchrotron radiation at beamline 12ID-B of the Advanced Photon Source (APS) at Argonne National Laboratory. The sample temperature was controlled using a Linkam hot stage in conjunction with a cryogenic cooling unit (type FTIR600) with a temperature programmer (type TMS94) also made by Linkam Scientific Instruments. Standard DSC aluminum pans with ~4 mg of samples were used. Patterns during isothermal crystallization were recorded by first melting at 120 °C for 5 min and cooling down to the crystallization temperature at a rate of 100 °C/min using liquid nitrogen in the coil of the stage. From T_c, a series of simultaneous two-dimensional (2D) SAXS/WAXD patterns were collected with time until the sample achieved complete transformation. The sample to SAXS detector distance was 4 m and 43 cm to the WAXD detector, and the exposure time was set to 0.1 s to minimize radiation damage. The 2D WAXD patterns were azimuthally averaged to one-dimensional patterns. WAXD intensities are shown as a function of the scattering vector, q ($q = 4\pi \sin\theta/\lambda$, where 2θ is the scattering angle and λ = 0.8856 Å is the wavelength of the 14 keV energy probing X-ray), measured in the range of 0.004−2.63 $Å^{-1}$. Q ranges were calibrated using silver behenate and the absolute intensity was calibrated using glassy carbon.

The spherulitic linear growth rates were measured using an Olympus BX51 polarized optical microscope fitted with an Olympus DP72 fast digital camera. Isothermal spherulitic growth was recorded and analyzed using the cellSens software commercialized by Olympus. The sample temperature was controlled using the same cryogenic Linkam hot stage used for the FTIR work. Growth rates (G) were obtained from the slope of the linear variation of the radius of the spherulites with crystallization time at a constant crystallization temperature. At least three different spherulites were measured. The average G and standard deviation were recorded at each T_c.

RESULTS AND DISCUSSION

Range of Crystallization Temperatures for Form I and Form II. Figure 1 displays the melting peaks of the polyacetals after isothermal crystallization at the indicated temperatures (T_c). The observed behavior is general for this series. Crystals formed in the low-T_c region melt at 5−8 °C lower temperatures than those formed in the high range of T_c. The transition from low to high melting point, which is highlighted by the red DSC traces in Figure 1, occurs within an extremely narrow change in T_c, less than 0.5 °C for PA-18, PA-19, and PA-23. The temperature at the transition coincides with the temperature at which a fast melt-recrystallization event from

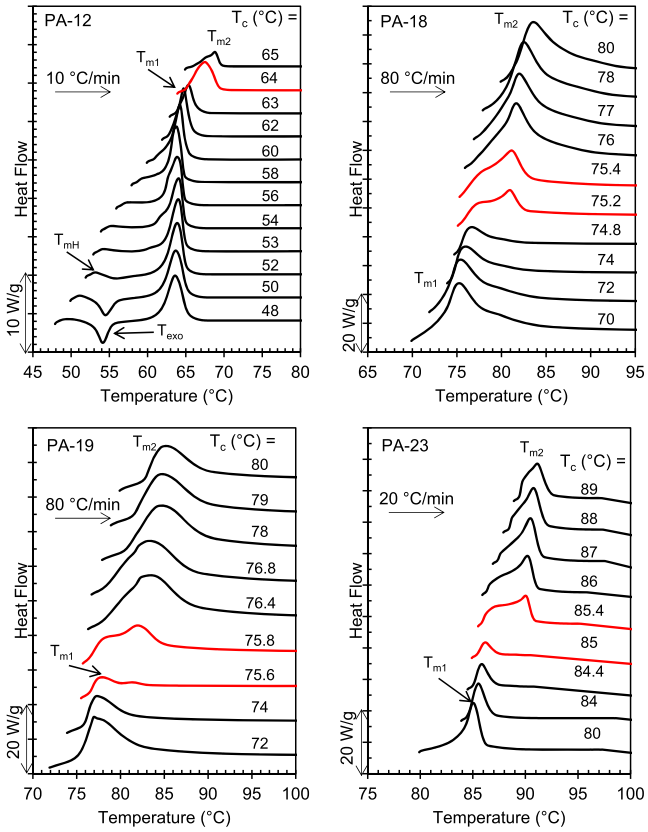

Figure 1. Melting curves of PA-12, PA-18, PA-19, and PA-23 after isothermal crystallization at temperatures indicated. The transition from low-melting-point Form I crystals to high-melting-point Form II is indicated by the red thermograms. Crystals of PA-18 and PA-19 were heated at 80 °C/min to minimize melting-recrystallization, while rates of 10 and 20 °C/min for PA-12 and PA-23, respectively, are sufficiently high as to avoid the recrystallization event.

Form I to Form II crystals takes place on heating rapidly formed crystals. As shown in the preceding work, in the same transition range of Figure 1, the initial crystals of Form I melt and recrystallize into more stable Form II crystals that, on further heating, melt at higher temperatures.[1] WAXD patterns collected during heating identified this polymorphic transition. Hence, the sharp change in melting point with increasing T_c shown in the thermograms of Figure 1 is consistent with the formation of Form I in the low range of isothermal T_c and formation of Form II in the high T_c range, below and above the red thermograms, respectively. Following previous studies, to minimize or avoid transformation of Form I to Form II on heating, the thermograms of Figure 1 were recorded at heating rates of 80 °C/min (PA-18 and PA-19) and at 10 or 20 °C/min for PA-12 and PA-23, respectively.

The exotherm observed for PA-12 at T_c between 48 and 52 °C in Figure 1 is explained by the formation of mixed hexagonal and Form I crystals at temperatures below 52 °C, as shown previously.[1] The hexagonal crystals melt at 50−52 °C and recrystallize at 54 °C into Form I, which melts further at 64 °C. From the thermograms of Figure 1, pure Form I crystals of PA-12 form in the range 56 °C < T_c < 64 °C, and pure Form II crystals form very slowly at T_c > 64 °C. These data point to a correlation between the formation of Form II and the length of the methylene spacer. When the distance between acetals reaches ≤12 CH_2, the transition from Form I to Form II occurs near the melting point of Form II, and such low

https://dx.doi.org/10.1021/acs.macromol.0c01443
Macromolecules 2020, 53, 7899−7913

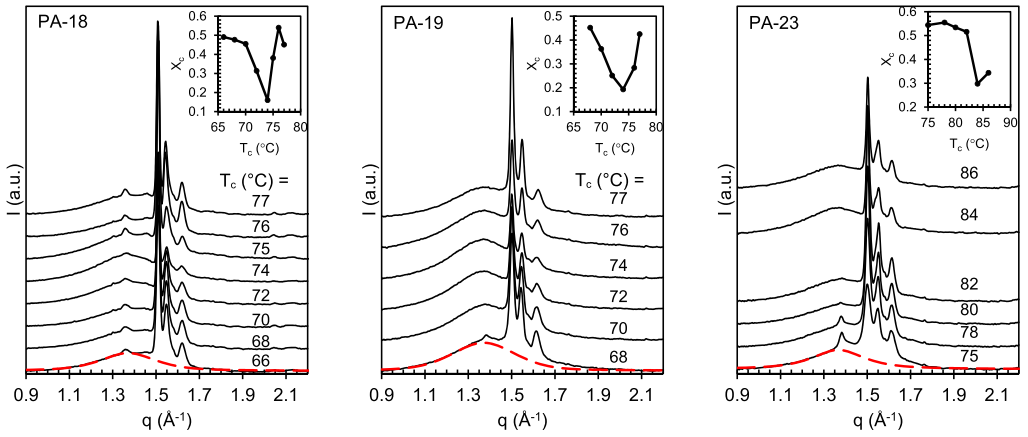

Figure 2. WAXD patterns collected at the indicated isothermal crystallization temperatures (T_c) for PA-18, PA-19, and PA-23. The scaled amorphous halo is shown in red for one of the patterns. The insets display the variation of degree of crystallinity with T_c.

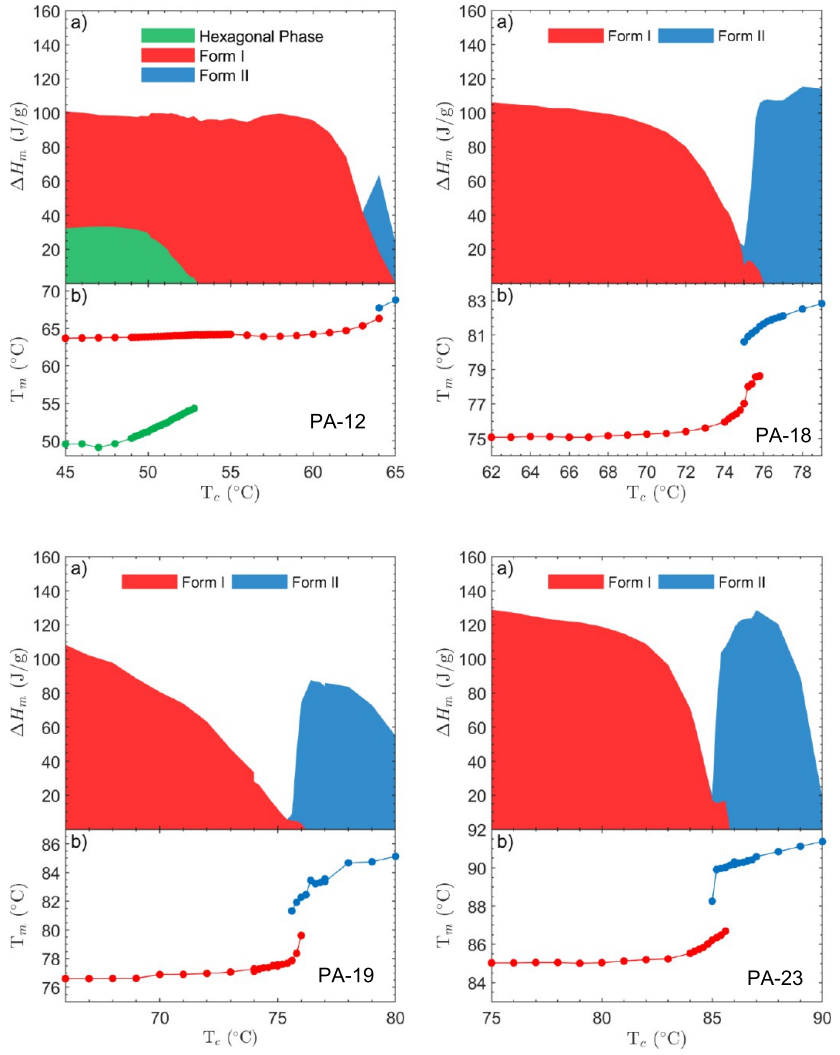

Figure 3. (a) Change in heat of fusion (ΔH_m) and (b) melting temperature (T_m) with increasing isothermal crystallization temperature for long-spaced polyacetals. Different colors represent data for hexagonal (green), Form I (red), and Form II (blue) phases.

undercooling makes crystallization of Form II a very slow process.

The sharp increase in melting temperature and associated change in crystal packing within a narrow decrease in undercooling for the polyacetals of Figure 1 are analogous to the behavior of precision polyethylenes with pendant Cl or Br atoms. The latter also transition within a 1−3 °C increase in T_c from a low melting point, *all-trans* planar crystal structure (Form I) to a more stable herringbone structure (Form II) that melts at higher temperatures.[36−38] Hence, it appears that the

https://dx.doi.org/10.1021/acs.macromol.0c01443
Macromolecules 2020, 53, 7899−7913

inception of polymorphism with increasing T_c and the associated effect of a sharp increase in the melting points are general features of most precision polyethylene-like systems with moieties easily accommodated into layered crystallites.

WAXD patterns recorded at the isothermal crystallization temperature using synchrotron radiation also corroborate the change from crystalline Form I to Form II with increasing T_c in polyacetals, as shown in Figure 2 for PA-18, PA-19, and PA-23. As discussed in the preceding work,[1] the signature of the formation of Form II in odd-spaced polyacetals (PA-19 and PA-23) is a loss of the reflection at 1.38 $Å^{-1}$, while the patterns of even-spaced polyacetals are unchanged at temperatures below and above the polymorphic transition. In Figure 2, loss of the 1.38 $Å^{-1}$ reflection for PA-19 at T_c > 70 °C and for PA-23 at T_c > 82 °C confirms that Form I and Form II are also enabled under isothermal crystallization from the isotropic melt and not just on recrystallization upon heating a form of lower stability, as shown earlier.[1] By comparing Figures 1 and 2, one notices that the transition temperatures from Form I to Form II observed by WAXD are 3−5 °C lower than those found by DSC. This difference can be explained by a lower sensitivity of WAXD to resolve the 1.38 $Å^{-1}$ reflection characteristic of Form I at crystallization temperatures approaching the polymorphic transition.

The WAXD patterns of PA-18 and PA-12 at T_c below and above the DSC transition are unchanged despite the polymorphic change. Although unusual, this invariance of WAXD patterns for different polymorphs has also been found in poly(1,3-dioxolane), a short-spaced polyacetal that exhibits three polymorphs. The three polymorphs display different melting temperatures, different crystallization kinetics, and different morphologies. However, they all have the same WAXD patterns.[39] In all long-spaced polyacetals, the variation of the degree of crystallinity at complete transformation (X_c), extracted from the WAXD patterns, supports a polymorphic transition taking place at the T_c where the melting point was found to increase by DSC. These plots are added as insets to each panel of Figure 2. The minimum of X_c observed in odd- and even-spaced polyacetals coincides with the DSC transition of Figure 1 and indicates a drastic change in crystallization kinetics in a narrow T_c range.

The variation of the heat of fusion (ΔH) and the peak melting temperature (T_m) as a function of increasing T_c, after complete isothermal transformation, are given in the composites of Figure 3 for each of the polyacetals studied. The type of phase and heat of fusion that evolves at a fixed T_c are distinguished by different colors: hexagonal (green), Form I (red), and Form II (blue). At the fastest crystallization or lowest T_c, the heat of fusion of all polyacetals is the same, about 110 J/g, indicating that independent of the acetal content, all polyacetals develop the same level of crystallinity in Form I under relatively fast crystallization. Moreover, the most intriguing feature in Figure 3 is the steep drop in heat of fusion of Form I at the transition temperature between Form I and Form II, followed by a sharp increase in ΔH with a slight increase in T_c, during the evolution of pure Form II. The transition is also demarcated by the step increase in melting point. We emphasize that increasing time at T_c does not change the small ΔH value found at the transition or the level of crystallinity (Figure SI 1).

Comparing Figures 1 and 3, it is clear that the steep decrease in heat of fusion corresponds to T_c very near the melting temperature of Form I, where crystallization of this form is basically suppressed. At this critical transition temperature, the heat of fusion of polyacetals PA-18, PA-19 and PA-23 is extremely low, less than 10% of the total transformation for PA-19, and is independent of the crystallization time. Hence, in this narrow temperature interval, Form I does not develop beyond the early stages, and Form II does not develop at all. Increasing T_c by a fraction of a degree results in the vanishing of the heat of fusion of Form I, while the value for Form II increases sharply to high levels. These data suggest that the two high-temperature polymorphs of long-spaced polyacetals, Form I and Form II, have well-defined stability temperature intervals with minimal overlap, less than about one degree.

The unique extinguishing crystallization at the transition between both polymorphs observed in Figure 3 has not been seen in other polymer systems that also undergo polymorphic transformations. In the latter, retardation effects in overall crystallization kinetics have been found at the transition between the two overlapping phases, but the degree of crystallinity is usually not affected because the development of one form is slowly replaced by the second with increasing crystallization time or at increasing crystallization temperatures.[16−25] The interest in the most drastic data of Figure 3, such as the extremely low ΔH of PA-19 or PA-23 at the transition, is the lack of formation of Form II despite the low transformation level of Form I. We recall that such an extinguishing effect for productive crystal growth was predicted on the basis of self-poisoning in modeling the minimum observed in the rate of crystallization of *n*-alkanes with decreasing T_c at the transition temperature between once folded and extended-chain structures or between successive integer folded forms.[31,32]

The T_c region for coexistence between both forms is not as sharp for PA-12 as it is for the longer spaced polyacetals, and it is shifted to a range of crystallization temperatures where the kinetics of the formation of Form II for PA-12 are very slow. Collecting isothermal overall crystallization and heat of fusion data for Form II for this sample is unduly long for T_c > 65 °C, as shown by the narrow blue region in Figure 3. On the other hand, crystallization of PA-12 at relatively low temperatures allows formation of the hexagonal phase admixed with Form I. As shown in the figure, this range corresponds to T_c < 53 °C.

The lower plots of each panel in Figure 3 highlight the sharp discontinuous change in melting point with increasing crystallization temperature at the transition between polymorphs. This discontinuous melting variation with T_c is remarkably similar to the thermal behavior of precision polyethylenes with Cl and Br.[2,36−38] One could then argue that polyacetals may display analogous behavior and initially take the sharp increase in melting point as associated with differences in crystalline layer packing between both forms. Unfortunately, the molecular weight of the polyacetals studied in this work is too low, and any attempt to produce oriented crystals has been so far unsuccessful. We suggest that packing of the methylene runs may be similar to precision polyethylenes with halogens, and the major difference between Form I and Form II may reside in the intermolecular staggering of the acetal groups. Such sharp temperature boundaries as those indicated by the data of Figure 3 are unusual for crystalline polymers and must be due to the precise placement of the moiety and the length of the methylene spacer. In previous works, when different crystal polymorphs develop for a polymer with a change in crystallization temperature, the overlapping temperature range where both

https://dx.doi.org/10.1021/acs.macromol.0c01443
Macromolecules 2020, 53, 7899−7913

forms coexist is broad, usually several degrees. For example, polymorphs found by increasing temperature in a polyester derived from isomannide and succinic acid (termed M4), poly(propylene 2,5-furandicarboxylate) and polyhydroxypropionate, overlap in a >30 degree range.[19,40,41] Similarly, polymorphs found with increasing temperature in an aromatic polyketone, polybutylene adipate, or in polylactic acid coexist in a 5−10 degree range.[18,22,42]

Overall Crystallization Rates. To better understand the unusual extinguished crystallization at the sharp transition temperature between both forms, the overall crystallization kinetics are analyzed from the DSC exothermic heat flow evolved with time during isothermal crystallization. A set of thermograms with increasing T_c is given for each polyacetal in Figure 4. The thermograms of PA-18, PA-19, and PA-23

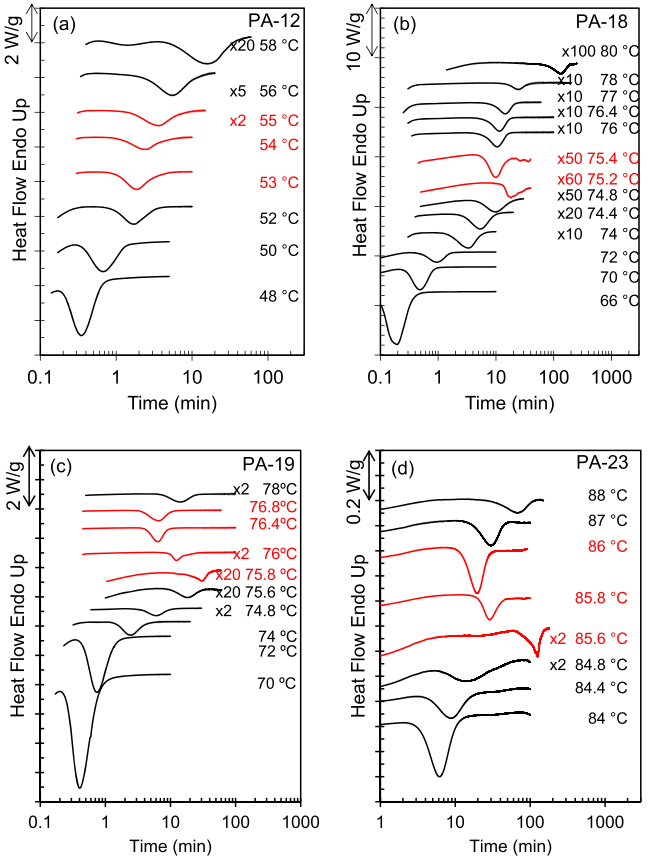

Figure 4. (a−d) Heat flow vs time during isothermal crystallization of PA-12, PA-18, PA-19, and PA-23 at the indicated crystallization temperatures. Selected exotherms are multiplied by the factors shown to emphasize the small heat flow at the transition between Form I and Form II (red thermograms).

display the same unusual evolution of heat flow with increasing T_c. Taking for example the exotherms of PA-18, increasing T_c from 66 to 75.2 °C in the range of formation of Form I, the crystallization time for full transformation increases from less than 1 to 50 min, as expected with decreasing undercooling following classical nucleation theory. At the transition temperature for PA-18 of 75.2 ± 0.2 °C, the heat evolved is so low that the actual exotherm had to be magnified 50−60 times to make it visible in the plots. The small exotherm corresponds to the very small value of the heat of fusion in Figure 3. Remarkably, contrary to expectations, with a very small increase in T_c, from 75.2 to 75.4 °C, the crystallization time decreases quite dramatically, from ∼50 to 20 min, and the area of the exotherm increases, denoting an inversion of crystallization kinetics at the transition between the two polymorphs. Upon increasing T_c further, in the range of formation of pure Form II, the time for crystallization progressively increases and now follows the expected kinetic variation with temperature. The same inversion of crystallization kinetics at the transition between the two crystal forms is found for PA-19 and PA-23 at higher T_c. Although an inversion is not evident, the rate for PA-12 is discontinuous at the transition between hexagonal and Form I (∼54 °C) phases. The exotherms for T_c at the transition between Form I and Form II of PA-12 cannot be recorded due to the slow kinetics, as mentioned earlier. The crystallization kinetics of PA-12 were acquired using FTIR to follow with time the evolution of a crystalline band, the rocking CH_2 progression mode at 850 cm^{-1} (Figure SI 2).

The thermograms of Figure 4 make relevant that the crystallization time of Form I reaches a maximum with increasing T_c. The time drops quickly at the inception of Form II and increases again with a further increase in T_c and the development of pure Form II crystallites. The transition temperatures where there is an inversion in the crystallization kinetics correspond to 85 ± 0.5 °C for PA-23, 75.6 ± 0.4 °C for PA-19, 75.2 ± 0.2 °C for PA-18, and 64.5 ± 0.5 °C for PA-12. The transition is highlighted by the red thermograms in Figure 4, which for PA-12 corresponds to the hexagonal-to-Form I transition.

The change in temperature where the polymorphic transition of long-spaced polyacetals evolves is very small, and the heat flow evolved so low that it becomes difficult to resolve the exotherms in this narrow T_c range. To extract quantitative kinetics of the independent evolution of Form I and Form II with a small change in undercooling, we used the endotherms obtained by melting from the isothermal crystallization temperature after increasing crystallization times. One example is given in Figure 5 for PA-23 crystallized in the transition region at T_c between 85 and 85.6 °C. The two melting peaks were deconvoluted to extract the evolution with time of Form I (low melting peak) and Form II (higher melting peak). The heat of fusion of Form I and Form II and the total heat of fusion are given as a function of time in the lower plots of Figure 5. At T_c = 85 °C, the transformation is completed in about 100 min, but the total heat of fusion is low; ΔH is only 20 J/g compared to >100 J/g obtained at lower T_c. Although a small content of Form I develops at this temperature, it strongly hampers the formation of Form II, only ∼2 J/g corresponds to Form II, and neither develop any further with prolonged crystallization time. With a slight increase in crystallization temperature (T_c = 85.2 °C), Form I develops first followed by Form II. At this temperature, the content of Form I remains low (∼20 J/g) and develops at a slower rate, as expected with decreasing undercooling. Conversely, Form II starts to develop after >100 min and increases at a very slow rate until a heat of fusion of ∼60 J/g. The half transformation time ($t_{0.5}$) for Form II is about 665 min, as shown. Increasing T_c to 85.4 °C, both forms start to develop at about the same time, although the heat of fusion of Form I remains low. The rate of evolution of Form II is much faster than at the lower temperature ($t_{0.5}$ = 192 min). At T_c = 85.6 °C, a very small content of Form I develops, and Form II develops at a much faster rate to reach ∼80 J/g. Pure Form II

https://dx.doi.org/10.1021/acs.macromol.0c01443
Macromolecules 2020, 53, 7899−7913

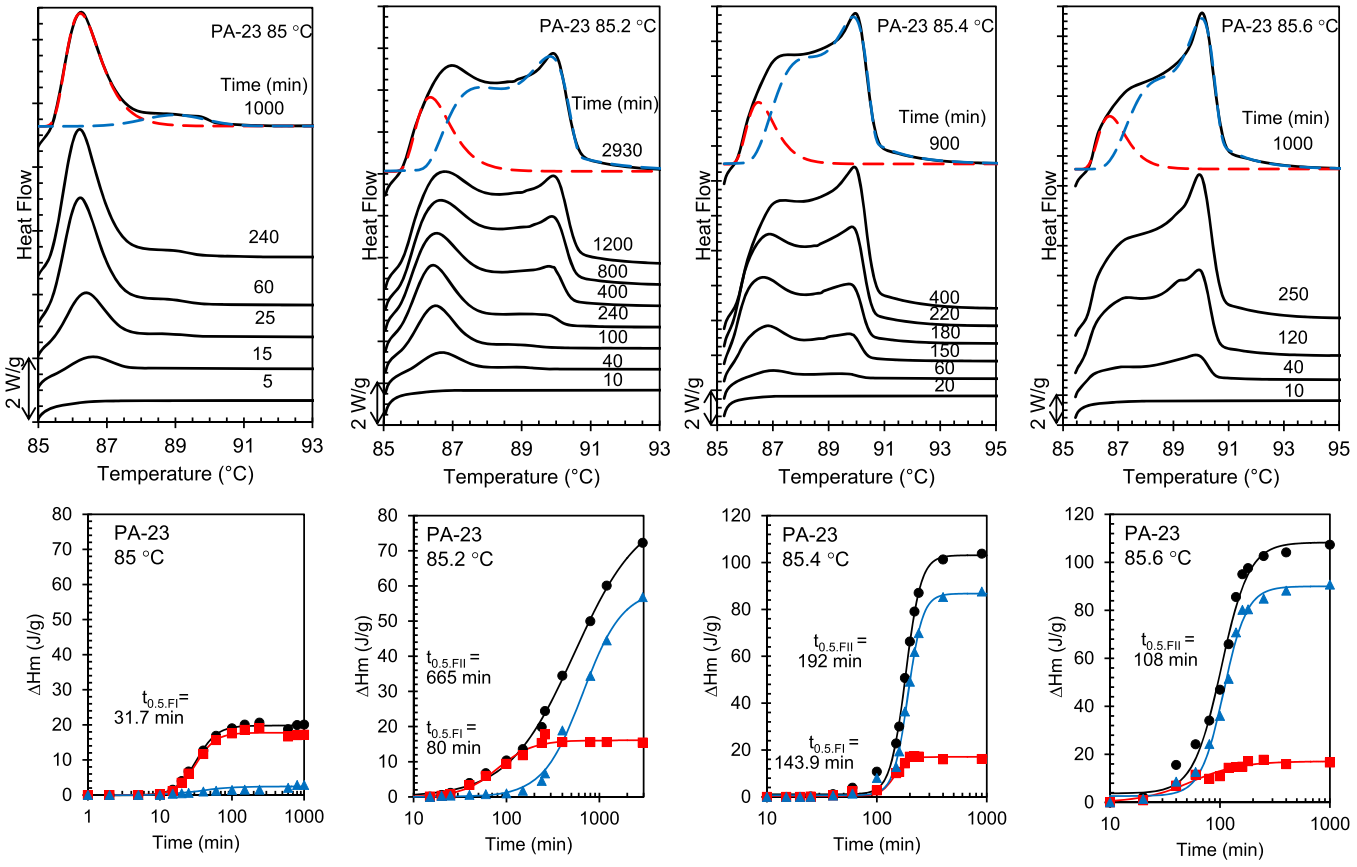

Figure 5. (Top) Melting endotherms of PA-23 crystallized at T_c for the indicated times. (Bottom) Variation of heat of fusion with time for Form I (red squares) and Form II (blue triangles) and total heat of fusion (black circles). Half crystallization times are indicated for each phase.

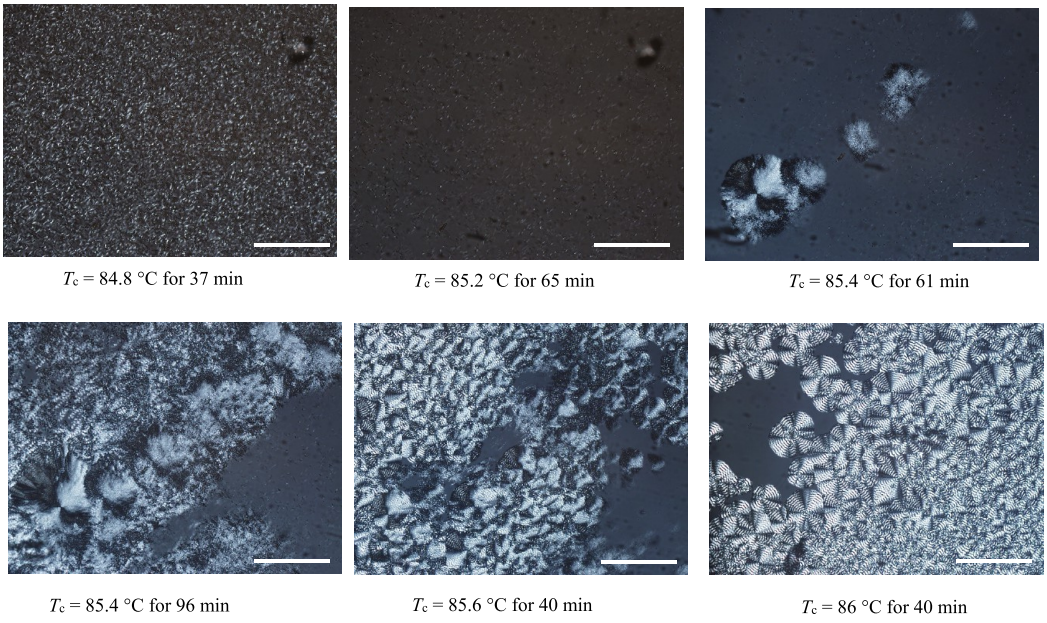

Figure 6. Morphological evolution at the transition between Form I and Form II of PA-23. Scale bars correspond to 200 μm.

develops at $T_c \geq 86$ °C. From the evolution of the heat of fusion in Figure 5, the $t_{0.5}$ of Form II at 85.6 °C is 108 min, in full agreement with the time at the maximum heat flow of the exotherm in Figure 4. It is remarkable that in this narrow range of crystallization temperatures, the crystallization rate of Form II increases with increasing temperature, and it is only when pure Form II develops that the rate of Form II follows the expected decrease with T_c. The data of Figure 5 serve to quantify the overall crystallization kinetics of Form I and Form II independently and also demonstrate that the growth of both forms overlaps in a very narrow range of T_c (<0.6 °C).

https://dx.doi.org/10.1021/acs.macromol.0c01443
Macromolecules 2020, 53, 7899−7913

The morphology at the transition between both forms was also followed by polarized optical microscopy. The set of representative micrographs shown in Figure 6 for PA-23 indicate a clear difference between the two forms, which is easily captured at the transition between Form I and Form II. Pure Form I develops up to T_c = 85 °C with a very high nucleation density. In this range of T_c, a profuse number of objects develop and impinge quickly. Between 85 and 85.2 °C, the nucleation density decreases and the axialitic objects stop growing after about 70 min. This very low birefringent morphology is unchanged with increasing time, reflecting the extinguished crystallization in this narrow range of T_c (Figure 3). At T_c = 85.4 °C, Form I nucleates first, as seen by the cluster of small dots in the lower right area of the image, and later, very few nuclei of Form II start to appear from areas mostly free of Form I. The morphology of Form II is clearly spherulitic with a well-defined Maltese cross and relatively fast growth. Additional asymmetric spherulites of Form II develop further with increasing time as they grow in between the small objects of Form I, as shown in the micrograph at the same T_c = 85.4 °C taken after 96 min. At T_c = 86 °C, only banded spherulites develop in pure Form II.

A feature that emerges from the images of Figure 6 is a clear difference in morphology, from small axialitic objects to large banded spherulites, and a drastic change in nucleation and growth at the transition between both forms. At any T_c < 85.5 °C, Form I has a high nucleation density even at one degree below its melting point and displays very slow growth (as shown by the images at 85.4 °C and in Figure SI 1). Conversely, around the transition, the nucleation rate of Form II is very low, but the growth rate is much faster compared with Form I. At T_c > 85.8 °C, when only pure Form II develops, the nucleation rate of Form II increases and, subsequently, for T_c > 86 °C, decreases with increasing T_c, thus following the expected temperature coefficient. Quantitative data demonstrating that such a large difference in nucleation between the polymorphs is due to differences in energy barriers are given and analyzed later. The question still remains as to why Form II does not develop at T_c = 85−85.2 °C while the level of crystallinity is so low.

Quantitative data of the overall rate of crystallization are given in Figure 7 where the natural logarithm of the rate is plotted as a function of crystallization temperature. Because the rates at each T_c for PA-18 and PA-19 are very similar, for clarity, the data are shown in two separate plots. Closed circles correspond to rates of Form I and open circles are for Form II. For T_c higher or lower than those at the transition range, the inverse of the time to peak, or minimum of the exotherms of Figure 4, is taken as the characteristic parameter of the overall crystallization kinetics ($1/t_{0.5}$). For T_c in the transition range, the rate is associated with the inverse of the time to reach 50% of the total transformation for each phase, which is extracted from the evolution of melting peaks with time, such as those shown in Figure 5. The data for PA-12 were obtained by DSC and FTIR, thus allowing measurements in a broad range of T_c including formation of the hexagonal phase (open diamonds), pure Form I, and pure Form II, as indicated in Figure 7a.

For all long-spaced polyacetals, the overall crystallization rate of Form I displays the usual negative temperature coefficient with very steep slopes at T_c 1−2 degrees below the observed melting point of Form I, which is near the vertical dashed lines in Figure 7. Conversely, with decreasing T_c, the crystallization rates of Form II first increase, reach a maximum

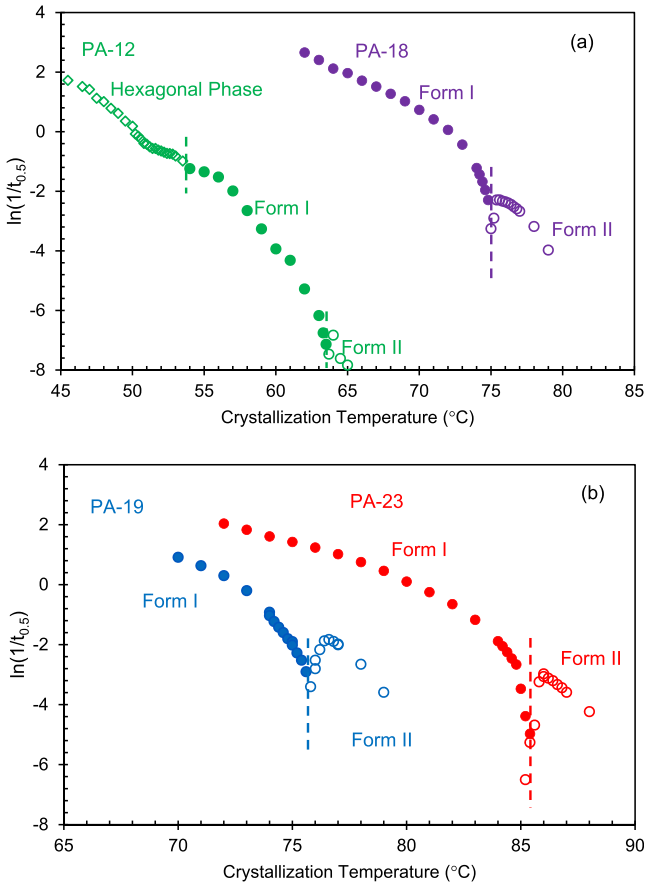

Figure 7. (a, b) Natural logarithm of the crystallization rate, represented by the inverse of half the crystallization time ($1/t_{0.5}$ with the time measured in minutes), vs crystallization temperature for PA-12, PA-18, PA-19, and PA-23. The crystallization rate minima at the transition between phases are demarked by vertical dashed lines. Open symbols are data for Form II, filled symbols correspond to Form I, and the open diamonds are data in the temperature region of formation of the hexagonal phase.

at T_c very close but above the melting point of Form I, and decrease rapidly when entering the narrow transition where both forms compete. As shown in Figure 7, the deep decrease in the overall crystallization rate of Form II at T_c only 0.2−0.5 °C below the observed maximum is so dramatic for PA-23, PA19, and PA-18 that any productive growth of Form I or Form II stops, as shown earlier. The inversion of the temperature gradient of the rate of Form II is also apparent for PA-12, although only four data points were collected in the range of formation of Form II. Moreover, a clear discontinuity in the temperature coefficient of the rate of PA-12 appears at ∼53 °C when entering the T_c region of formation of the hexagonal phase from above. The general observation from the data of Figure 7 is that a minimum or inversion in the crystallization rate at temperatures in the transition between two crystal structures is not an isolated case for halogen-containing precision polyethylenes.[2] Besides the appearance of the minimum in other polymorphic systems,[19,20,22,26−28] this feature appears as a more general case of polyethylene-like structures with moieties that can be accommodated in crystalline layers due to a equidistant placement along the backbone.

The characteristics of the deep rate minima of Figure 7 resemble the feature of self-poisoning observed in *n*-alkanes

https://dx.doi.org/10.1021/acs.macromol.0c01443
Macromolecules 2020, 53, 7899−7913

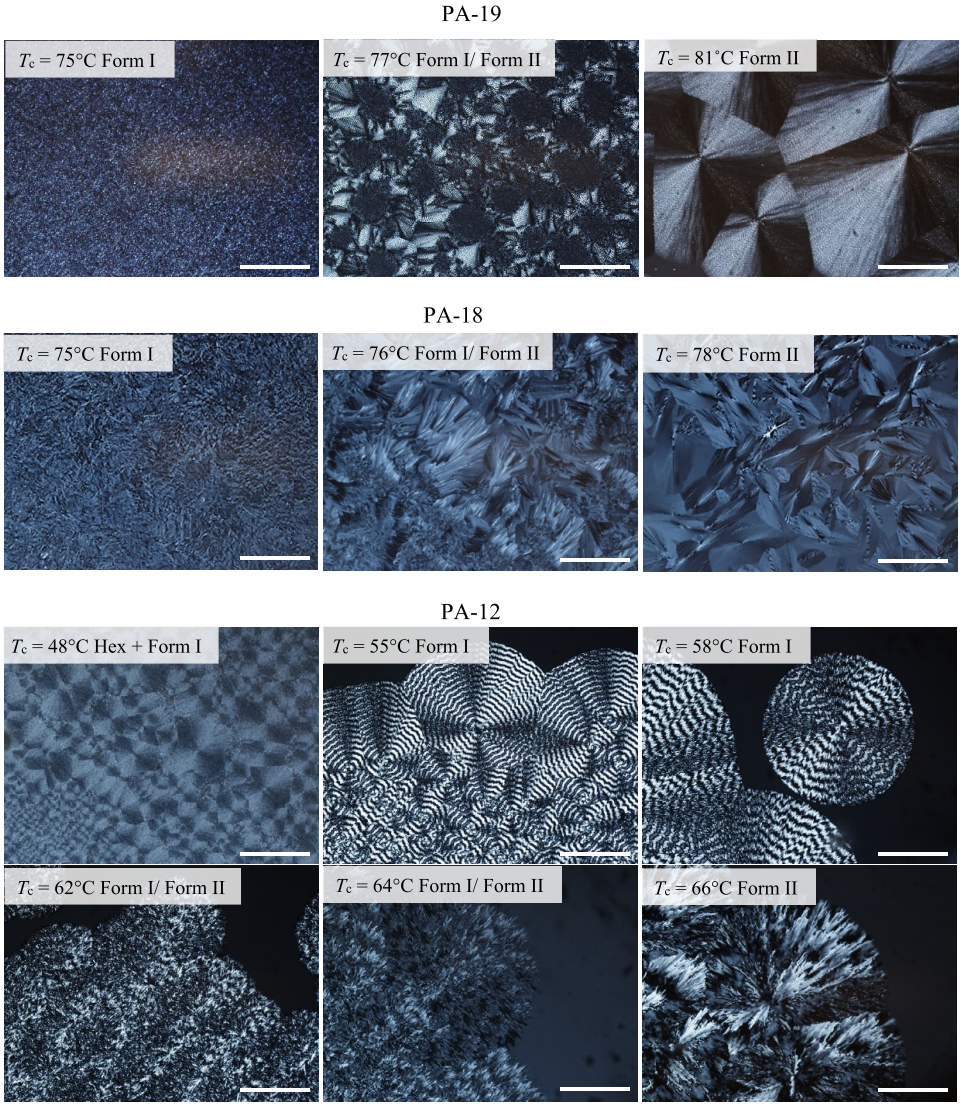

Figure 8. Representative polarized optical micrographs of PA-19, PA-18, and PA-12 below, at, and above the polymorphic transitions at the indicated isothermal crystallization temperatures. Scale bar correspond to 200 μm.

and, more recently, in precision polyethylenes with Br.[2,32] In the proposed self-poisoning mechanism, chains wrongly attached to a crystal surface will hinder further growth until they detach or reorganize into the correct chain structure. The surface blocking effect in precision polyethylenes with Br by Form I on the growing surface of Form II is very pronounced at temperatures approaching the melting point of Form I from above.[2] The kinetic data of Figure 7 could be explained in an analogous manner. Taking PA-23 as an example, the reason for Form II not to develop at T_c = 85 °C and to develop gradually at higher rates up to T_c = 86 °C could also be a strong poisoning effect of Form I on Form II (Figures 5 and 6). This poisoning effect may be very strong for the initial nucleation of Form II such that at 85 °C, Form I competes with the formation of nuclei of Form II and effectively suppresses any nucleation event or productive growth in Form II. At the same time, growth of the kinetically favored Form I is very slow due to the low undercooling for this phase. At increasing temperatures, the probability of any segments of Form I hampering the development of Form II nuclei diminishes, and the level of crystallinity of Form II starts to increase up to T_c = 86 °C. At higher T_c (at or above the melting point of Form I), any inference from Form I on the nucleation or growth of Form II ceases, and the crystallization rate kinetics follow the usual negative temperature coefficient.

While preferential self-poisoning at the nucleation step of Form II could indeed explain the observed deep minimum in the overall crystallization rate of long-spaced polyacetals, such rate inversion could also be explained just by differences in kinetics between both forms. For example, a lower free energy barrier for nucleation (ΔF_n^*) of Form I could explain why this form nucleates faster than Form II even at temperatures so close to its melting point, thus hindering nucleation and growth of Form II until nucleation of Form I is totally suppressed. Large differences in ΔF_n^* also explain the narrow temperature range where the minimum is observed and the fact that the inversion of the rate of Form II with decreasing temperature is found only when both forms coexist, rather than at T_c above the melting point of Form I, as was the case for systems with Br.

Because the premise of the proposed self-poisoning mechanism is a surface blockage effect, the major experimental evidence is retardation in the growth rate of the most stable form, usually observed in the linear spherulitic growth[2,33] or in

https://dx.doi.org/10.1021/acs.macromol.0c01443
Macromolecules 2020, 53, 7899−7913

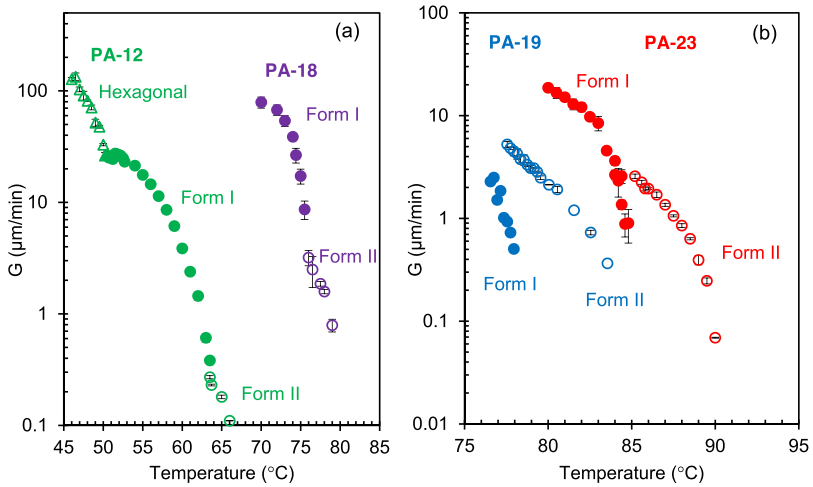

Figure 9. Variation of the logarithm of the linear growth rates with increasing isothermal crystallization temperature of hexagonal (open triangle), Form I (solid circle), and Form II (open circle) phases of (a) PA-12 (green) and PA-18 (purple) and (b) PA-19 (blue) and PA-23 (red). Standard deviations from the mean values are indicated.

the growth of a specific crystallographic plane,[32] at temperatures approaching from above the melting point of the kinetically favored structure. Hence, linear growth rates were obtained to probe if minima are also observed in the growth rates of Form II of long-spaced polyacetals at temperatures approaching the melting point of Form I from above. Such an experimental feature would be in consonance with the characteristics of the self-poisoning effect. Prior to presenting those data, the morphology of each phase is first differentiated by optical microscopy for all polyacetals. Large morphological differences between both forms allow independent quantitative determination of the linear growth rates of each form at a fixed T_c.

Overall Morphology and Isothermal Linear Growth Rates. The dramatic effect on overall crystallization rate at the transition between Form I and Form II is accompanied by a morphological change, as was indicated in Figure 6 for PA-23. Such a change in morphology is also present with very similar features in PA-19 and PA-18 and in the characteristics of the spherulites of PA-12. Representative polarized optical micrographs are given in Figure 8 at temperatures of formation of pure Form I, at the transition where both forms coexist, and above the transition for pure Form II. Except for PA-12 that develops spherulites in the whole range of T_c, all other polyacetals develop profuse nucleation of irregular objects in the range where Form I develops. At temperatures approaching the transition, slowly growing open axialites of Form I can be identified, thus allowing growth measurements of this form. Conversely, highly birefringent positive spherulites develop for Form II even at the transition temperatures between both phases, as shown in Figure 6. The images of PA-19 at 77 °C are also examples of the nucleation and fast growth of Form II as banded spherulites subsequent to the formation of a cluster of low birefringent highly nucleated Form I. At T_c > 78 °C, above the transition, the view is fully covered with large spherulites of Form II. The change in morphology from highly nucleated objects to spherulites is also apparent in the images of PA-18, but the morphological features of Form II resemble those of low-molar-mass polymers. Although GPC data gave similar molecular weights for PA23, PA-19, and PA-18, from the flow behavior, the apparent melt viscosity of PA-18 is lower than the rest of the polyacetals studied. A low molecular weight could explain the lack of banding and the elongated appearance of some of the spherulites of PA-18.

We choose a larger set of images for PA-12 in Figure 8 to illustrate the two polymorphic transformations. At T_c < 52 °C, PA-12 develops a very low birefringent spherulitic mixture of hexagonal and Form I structures, as shown in the image at 48 °C. In the range of pure Form I, the spherulites become banded and highly birefringent with the expected increase in band width spacing with temperature (images at 55 and 58 °C). The transition from Form I to Form II in the 62−64 °C range occurs with a deterioration of the internal symmetry of the spherulites. At the transition, the spherulites lose the characteristic Maltese cross and most banding features as a consequence of the simultaneous nucleation and growth of both phases. Pure Form II develops very slowly at T_c > 64 °C; hence, the spherulites are more open and again highly birefringent, as exemplified by the image taken at 66 °C after 3900 min crystallization.

A feature of interest is the double-banded spherulites of Form II found in odd-spaced polyacetals (PA-23 and PA-19), which is indicative of a strongly biaxial crystal structure. It is feasible that in Form II, the PA molecules bend at the acetal group, similar to the zigzag structure found in Cl- and Br-substituted precision polyethylenes.[36−38] Bending may differently affect the even-spaced polyacetals and could explain the lack of banding in the spherulites of Form II of PA-12 and PA-18.

The variation of the linear growth rates with increasing crystallization temperature is given in Figure 9a for PA-12 and PA-18 and in Figure 9b for PA-19 and PA-23. As for the overall crystallization, closed circles are data for Form I and open circles correspond to Form II. The open triangles for PA-12 are data in the T_c region where hexagonal and Form I structures coexist. Because the overlapping temperature range between Form I and Form II is so narrow, Form I melts basically at the polymorphic transition (see Figure 1), and any rate minima for Form II consistent with self-poisoning are expected at or very near the transition as well. However, no minima are observed for the growth rates of Form II at crystallization temperatures approaching the melting point of Form I in any of the data of Figure 9. Instead, in the range of temperatures where the growth of both forms can be measured

https://dx.doi.org/10.1021/acs.macromol.0c01443
Macromolecules 2020, 53, 7899−7913

at the same T_c, the growth rate of Form II is much faster than growth of Form I, as was implicit from the optical micrographs of Figure 6. We should point out that the experimental uncertainties in the measurements of growth for Form II are low, smaller than the symbol size in the figure for most data, but larger for Form I, especially for the data in the transition region due to the low birefringent small axialites of Form I for these polymers at temperatures near the melting point of Form I. The exception is data for Form I of PA-12 where the uncertainty remains low. The growth rates of PA-18, PA-19, and PA-23 display the usual negative temperature coefficient for Form I and Form II.

Since no minima with decreasing T_c are observed in the growth rate data of Form II in any of the polyacetals, we need to conclude that in these systems, self-poisoning, if operative, will be preferential to the nucleation of Form II and at temperatures close to the melting point of Form I. The rationale for observing a minimum consistent with self-poisoning in the growth rates of polyethylenes with bromine[2] and not in the polyacetals is the following. In polyethylenes with Br, we observed mixed Form I and Form II in a narrow range of temperatures (2−3 °C). However, because Form I melts at 10 degrees above the inception of Form II, the growth of Form II at temperatures approaching the melting point of Form I from above is sufficiently slow for a detectable retardation by a wrong conformation temporarily attached at the growth front of the herringbone structure. In polyacetals, the difference between inception of Form II and melting of Form I is too narrow, less than one degree. In the transition, at temperatures where we first observe nucleation of Form II of polyacetals, the growth of this form is much faster than any possible attachment of Form I, and any effect on growth of Form II is negligible. There is also the possibility that self-poisoning affects preferentially one crystal face, as it was demonstrated for long-chain *n*-alkanes,[43] and may not show up in the measured spherulitic growth rates of the polyacetals.

On combining the morphological evidence from Figures 6 and 8 with the growth data of Figure 9, it becomes evident that Form I is kinetically favored as it develops in the low temperature range, with probably a very low energy barrier for nucleation. Hence, even at very low undercooling, for example, T_c = 84−85 °C for PA-23, the nucleation events of Form I remain high, while growth becomes very slow at temperatures approaching the melting point of this phase. Form II is thermodynamically more stable as it develops and melts at higher temperatures. The reduced number of nuclei leading to highly birefringent, banded spherulites of Form II is consistent with a harder to nucleate unit cell. In the range of T_c of coexistence of both forms, the nucleation of Form I is still profuse despite the extremely low undercooling, while nucleation of Form II is frustrated and competes with nuclei of Form I even when it develops at the highest undercooling (highest drive) for this phase, as shown in Figure 6 for PA-23. Hence, although the effect of self-poisoning during nucleation of Form II in the coexistence region cannot be ruled out, large differences in nucleation barriers between both forms, and the slow growth of Form I, explain the low degree of crystallinity that developed just before the transition to Form II.

The growth rate data at the transition between Form I and the hexagonal phase of PA-12 in Figure 9a are of interest because the data for Form I display a true inversion in the range of temperatures between 50 and 52 °C. In other words, a minimum of the crystallization rate is observed for Form I of PA-12 when approaching the melting point of the hexagonal form from above, which is consistent with the self-poisoning effect on the growth of Form I. There are two major differences between the transition from the hexagonal phase to Form I and that from Form I to Form II that explain why the effect of self-poisoning in the rate is observed in the first but not in the second transition. First of all, the temperature range of coexistence between the hexagonal phase and Form I is broader, as shown in Figure 3, and in addition to a different packing, the transition between the hexagonal phase and Form I carries an increase in lamellae thickness by one repeating unit. Hence, there is a change in lamellae thickness as in *n*-alkanes,[32] while there is no change in crystal thickness below and above the Form I-to-Form II transition.[1] It appears that in analogy with the behavior of *n*-alkanes, a mismatch in stem length between Form I and the hexagonal crystals makes for a stronger retardation at the growth front of Form I by temporal depositions of the shorter hexagonal phase. Such a temporal blockage causes a decrease in the growth rates of Form I of PA-12 at temperatures close to but above the melting point of the hexagonal phase (see Figure SI 3 for expansion of the growth rate data of PA-12 in this region).

The free energy barrier for nucleation of Form I and Form II can be estimated from the analysis of the growth rate data according to the coherent surface nucleation theory.[44,45] The linear growth rate can be described as

$$G = G_o e^{-(U^*/R(T-T_\infty))} e^{-(\Delta F_n^*/RT)} \quad (1)$$

The pre-exponential term G_o involves all terms weakly dependent on temperature, while $U^*/R(T - T_\infty)$ is the term associated with segmental transport across the crystal-liquid interface. It is formulated taking the Vogel−Fulcher−Tamann−Hesse expression to describe the effective activation energy for segmental transport in the crystallization process.[46−48] T_∞ represents the temperature below which the required segmental motion becomes infinitely slow, usually taken 30−50 K below T_g ($T_\infty = T_g - C_2$). Although the values of U^* and T_∞ are unknown, the two sets most often used in analysis of crystallization kinetics are U^* = 1500 cal/mol and C_2 = 30° and U^* = 4120 cal/mol and C_2 = 51.6°. ΔF_n^* is the height of the free energy barrier that must be surmounted to form a stable nucleus. For a nucleus formed by deposition of monomolecular layers on a surface

$$\Delta F_n^* = \frac{4b\sigma_e\sigma_u T_m^o}{\Delta H \Delta T} \quad (2)$$

Here, b is the width of the depositing stem, and σ_e and σ_u are the basal and lateral surface free energies, respectively. ΔH is the latent heat of fusion. The linear form of the growth rate equation gives

$$\ln G + \frac{U^*}{R(T - T_\infty)} = \ln G_o - \frac{K_g T_m^o}{T\Delta T} \quad (3)$$

with K_g defined as $K_g = \frac{4b\sigma_e\sigma_u}{R\Delta H}$ for the formation of a two-dimensional nucleus.

The energy barrier for nucleation (ΔF_n^*) can be determined from the slope (K_g) of the experimental ln G data plotted vs ($\frac{T_m^o}{T\Delta T}$) according to eq 3, $\Delta F_n^* = (K_g R T_m^o)/\Delta T$.

This analysis requires knowledge of the equilibrium melting temperature of each polyacetal for each crystalline form (T_m^o).

https://dx.doi.org/10.1021/acs.macromol.0c01443
Macromolecules 2020, 53, 7899−7913

The equilibrium melting temperatures of Form II were obtained from T_m/T_c extrapolations after isothermal crystallization at low levels of crystallinity, according to the Hoffman–Weeks approximation (Figure SI 4).[49] Due to the fast melting-recrystallization of Form I, this method could not be applied and T_m^o for Form I was approximated by the final melting point of Form I from the data of Figure 1. These data correspond to the end of the transition or the temperature at which no Form I crystals were observed. The estimated equilibrium melting temperatures, including the most possible range of values for Form I, are listed in Table 2.

Table 2. Equilibrium Melting Temperatures of Form I and Form II (T_m^o) and Values of the Slopes ($-K_g$) from Figure 11

polyacetal	crystal form	T_m^o (°C)	$-K_g$ (K)
PA-12	Form I	65.5 (64)[a]	17.6 (8.7)
	Form II	70	[b]
PA-18	Form I	79 (77)[a]	13.5 (4.6)
	Form II	85.3	27
PA-19	Form I	81 (79)[a]	15.7 (3)
	Form II	89.5	32.2
PA-23	Form I	88 (86)[a]	14 (5.3)
	Form II	95	34

[a]Highest and lowest estimates of T_m^o for Form I from DSC melting endotherms after isothermal crystallization (Figure 1). [b]Insufficient experimental data.

With the T_m^o values of Form II and the highest estimates for Form I, the experimental linear growth rates are compared for the same undercooling ($\Delta T = T_m^o - T_c$) in Figure 10. The

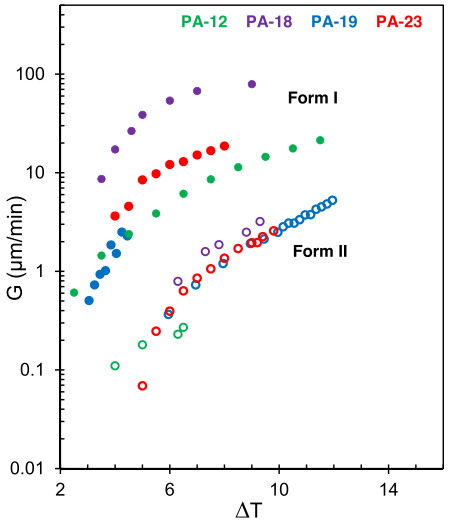

Figure 10. Variation of the logarithm of the linear growth rates with undercooling ($\Delta T = T_m^o - T_c$). Open symbols are G data for Form II. Filled symbols are data for Form I.

most important feature of this figure is that on the basis of undercooling, the growth rates of Form I are at least 10 times faster than for Form II. This difference is maintained if the overall crystallization rates are plotted as a function of undercooling. Also of interest is the collapse of the growth rate data for Form II of all polyacetals into the same line. The normalization of the rates by undercooling is indicative of the same type of nucleation and growth in Form II for these long-spaced polyacetals. The scattering of the few data for Form II of PA-12 is due to a larger experimental error in the growth measurement at the lowest undercooling and the higher values for PA-18 to the lower molecular weight, as mentioned. The growth rates of Form I are more scattered due to larger experimental error in the growth measurement of this phase. The use of a lower T_m^o for Form I further increases the difference in growth rate between Form II and Form I at a fixed undercooling.

To confirm that the large difference in growth rates between Form I and Form II is associated with similarly large differences in the free energy barrier for nucleation, the rates are plotted according to eq 3 in Figure 11. Due to the small

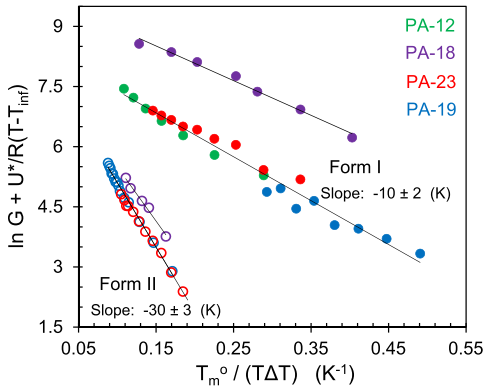

Figure 11. Analysis of the temperature coefficient of the growth rate kinetics of long-spaced polyacetals according to surface nucleation theory (eq 3). Open symbols correspond to data for Form II. Closed symbols are data for Form I.

number of data of Form II for PA-12 and larger uncertainties, these data are excluded from Figure 11. The data in this figure were calculated with $U^* = 1500$ cal/mol, $C_2 = 30$ K, $T_g = -80$ °C, and a value for T_m^o of Form I intermediate in the range listed in Table 2. Except for the data of PA-18 that are for both forms displaced to higher values, the temperature coefficient of the rate data collapses to a single behavior with slopes for Form II that are three times higher than the values of Form I. The choice of a lower or higher T_m^o of Form I within the range will change the absolute value of the slope, but the characteristic linearity of the gradient and the fact that the slopes of Form II are much higher remain unchanged. The same linearity and same difference between slopes of data from Form I and Form II will be obtained if a different constant transport term is used. The displacement of the data for PA-18 is attributed to the suspected lower molecular weight. If a lower value for U^* is used for this polyacetal, as would correspond to a less viscous melt, then the data for PA-18 in Figure 11 will also collapse with the data of the other polyacetals.

Since the slope ($-K_g$) of Figure 11 is proportional to the free energy barrier for surface nucleation, the same difference is expected. This is shown in Figure 12 where calculated values of ΔF_n^* are plotted as a function of undercooling for Form I and Form II. With the mean estimate for T_m^o of Form I used for the data shown in Figure 12, the energy barrier to be surmounted for surface nucleation of Form II is three times the barrier for Form I. If we consider the interval of uncertainty for the T_m^o of Form I and assuming the same ratio between the barriers of Form II and Form I for primary and secondary nucleation,

https://dx.doi.org/10.1021/acs.macromol.0c01443
Macromolecules 2020, 53, 7899–7913

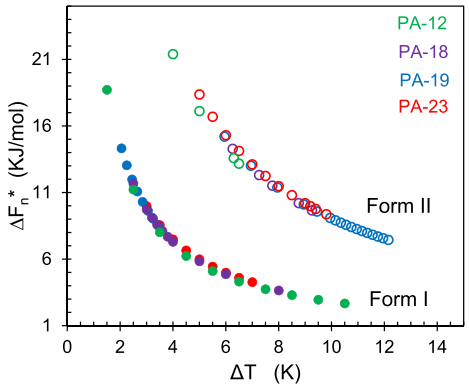

Figure 12. Free energy barrier for nucleation vs undercooling ($\Delta T = T_m^o - T_c$) for long-spaced polyacetals. Open symbols are data for Form II. Filled symbols are data for Form I.

then we conclude that the nucleation barrier for the formation of Form II is 2−6-fold higher than for Form I, in agreement with the observed morphological differences and growth rate data of both phases.

CONCLUSIONS

Long-spaced polyacetals with structural repeating unit $-[O-CH_2-O-(CH_2)_x]_n-$ and x = 12, 18, 19, or 23 crystallize from the melt in different layered polymorphs as a function of increasing crystallization temperature. Under isothermal crystallization, these polyacetals develop Form I, a kinetically favored phase in the lower range of crystallization (T_c), and Form II, a thermodynamically more stable form in the highest T_c range. A hexagonal packing also develops isothermally for PA-12 in the lowest T_c range.

Crystals in Form I and Form II are easily distinguished by a 5−8 degree difference in melting points and characteristic morphological features. The profuse nucleation of Form I in PA-18, PA-19, and PA-23 leads to small axialitic objects that contrast with the large, highly birefringent spherulites of Form II, which nucleate more sporadically. Form I and Form II coexist in an unusually narrow range of temperatures (<1 degree) where with increasing T_c, the melting point increases sharply when transitioning from Form I to Form II.

A peculiar feature of the crystallization of these polyacetals is the extremely low degree of crystallinity developed at the transition between Form I and Form II. While crystallization in each form can reach high degrees of crystallinity, at the boundary between phases, the crystallization is basically extinguished. This unusual feature is attributed to large differences in the crystallization kinetics of both phases. Differences in nucleation and growth that explain the unusual kinetics were extracted by a combination of overall and linear growth rates measured by DSC and polarized optical microscopy.

The overall crystallization rates of Form I display the usual negative temperature coefficient with increasing T_c, reaching very low values at temperatures approaching the melting point of this form. A negative temperature coefficient also holds for the rates of Form II in the range of formation of the pure phase. However, when both forms coexist, the rate of Form II decreases drastically with decreasing T_c. The inversion of the overall crystallization rate of Form II correlates with a progressive decrease in nucleation density of Form II with decreasing temperature in the overlapping region due to a competition in nucleation between both forms. The nucleation of kinetically favored Form I is relatively high in the same temperature range.

The linear growth rates, measured independently for Form I and Form II, followed the usual negative temperature coefficient. While at a fixed temperature in the transition region, the growth rates of Form II are higher than those of Form I, at a fixed undercooling, the rates of Form I are at least one order of magnitude higher than for Form II. The latter is a consequence of the large differences in free energy barrier for nucleation between both forms. From the analysis of the temperature coefficient of the linear growth rates following surface nucleation theory, the energy barrier to surmount nucleation of Form II is two to six times higher than the barrier for nucleation of Form I.

A minimum in the growth rate of Form I of PA-12 consistent with the effect of self-poisoning is observed at temperatures approaching the melting point of the hexagonal phase from above. A stronger retardation effect at the growth front at temperatures above this polymorphic transition is explained by differences in stem length between the hexagonal and Form I crystals. Due to a narrower range of coexistence between Form I and Form II and no appreciable differences in lamellae thickness, the poisoning effect is not observed in the growth rates of Form II.

ASSOCIATED CONTENT

Supporting Information

The Supporting Information is available free of charge at https://pubs.acs.org/doi/10.1021/acs.macromol.0c01443.

Unchanged low heat of fusion of PA-23 with time at the lowest point in the transition and expanded polarized optical micrographs of Form I; crystallization kinetics of PA-12 followed by FTIR; expansion of the plot of linear growth rates as a function of T_c in the hexagonal−Form I region of PA-12; extrapolation of observed melting temperatures vs T_c (PDF)

AUTHOR INFORMATION

Corresponding Author

Rufina G. Alamo − *Department of Chemical and Biomedical Engineering, FAMU-FSU College of Engineering, Tallahassee, Florida 32310-6046, United States;* orcid.org/0000-0002-3061-499X; Email: alamo@eng.fsu.edu

Authors

Xiaoshi Zhang − *Department of Chemical and Biomedical Engineering, FAMU-FSU College of Engineering, Tallahassee, Florida 32310-6046, United States*

Stephanie F. Marxsen − *Department of Chemical and Biomedical Engineering, FAMU-FSU College of Engineering, Tallahassee, Florida 32310-6046, United States*

Patrick Ortmann − *Chemical Materials Science, Department of Chemistry, University of Konstanz, Konstanz 78457, Germany*

Stefan Mecking − *Chemical Materials Science, Department of Chemistry, University of Konstanz, Konstanz 78457, Germany;* orcid.org/0000-0002-6618-6659

Complete contact information is available at: https://pubs.acs.org/10.1021/acs.macromol.0c01443

Notes

The authors declare no competing financial interest.

https://dx.doi.org/10.1021/acs.macromol.0c01443
Macromolecules 2020, 53, 7899−7913

■ ACKNOWLEDGMENTS

This material is based on work supported by the National Science Foundation, Polymers Program, under grant DMR 1607786. P.O. and S.M. gratefully acknowledge the support by the Stiftung Baden-Württemberg. The help of Xiaobing Zuo (Argonne National Laboratory) with synchrotron experiments and of REU students, Sidney M. Cameron, and Michael Parkhurst with the collection of optical micrographs and measurement of growth rates is gratefully acknowledged.

■ REFERENCES

(1) Zhang, X.; Zuo, X.; Ortmann, P.; Mecking, S.; Alamo, R. G. Crystallization of Long-Spaced Precision Polyacetals I: Melting and Recrystallization of Rapidly Formed Crystallites. *Macromolecules* **2019**, *52*, 4934−4948.

(2) Zhang, X.; Zhang, W.; Wagener, K. B.; Boz, E.; Alamo, R. G. Effect of Self-Poisoning on Crystallization Kinetics of Dimorphic Precision Polyethylenes with Bromine. *Macromolecules* **2018**, *51*, 1386−1397.

(3) Sworen, J. C.; Smith, J. A.; Berg, J. M.; Wagener, K. B. Modeling Branched Polyethylene: Copolymers Possessing Precisely Placed Ethyl Branches. *J. Am. Chem. Soc.* **2004**, *126*, 11238−11246.

(4) Baughman, T. W.; van der Aa, E.; Wagener, K. B. Linear Ethylene - Vinyl Ether Copolymers : Synthesis and Thermal Characterization. *Macromolecules* **2006**, *39*, 7015−7021.

(5) Song, S.; Miao, W.; Wang, Z.; Gong, D.; Chen, Z.-R. Synthesis and Characterization of Precisely-Defined Ethylene-Co-Aryl Ether Polymers via ADMET Polymerization. *Polymer* **2015**, *64*, 76−83.

(6) Gaines, T. W.; Trigg, E. B.; Winey, K. I.; Wagener, K. B. High Melting Precision Sulfone Polyethylenes Synthesized by ADMET Chemistry. *Macromol. Chem. Phys.* **2016**, *217*, 2351−2359.

(7) Aitken, B. S.; Buitrago, C. F.; Heffley, J. D.; Lee, M.; Gibson, H. W.; Winey, K. I.; Wagener, K. B. Precision Ionomers: Synthesis and Thermal/Mechanical Characterization. *Macromolecules* **2012**, *45*, 681−687.

(8) Watson, M. D.; Wagener, K. B. Functionalized Polyethylene via Acyclic Diene Metathesis Polymerization: Effect of Precise Placement of Functional Groups. *Macromolecules* **2000**, *33*, 8963−8970.

(9) Opper, K. L.; Markova, D.; Klapper, M.; Müllen, K.; Wagener, K. B. Precision Phosphonic Acid Functionalized Polyolefin Architectures. *Macromolecules* **2010**, *43*, 3690−3698.

(10) Baughman, T. W.; Chan, C. D.; Winey, K. I.; Wagener, K. B. Synthesis and Morphology of Well-Defined Poly(Ethylene-Co-Acrylic Acid) Copolymers. *Macromolecules* **2007**, *40*, 6564−6571.

(11) Ortmann, P.; Trzaskowski, J.; Krumova, M.; Mecking, S. Precise Microstructure Self-Stabilized Polymer Nanocrystals. *ACS Macro Lett.* **2013**, *2*, 125−127.

(12) Busch, H.; Schiebel, E.; Sickinger, A.; Mecking, S. Ultralong-Chain-Spaced Crystalline Poly(H-Phosphonate)s and Poly-(Phenylphosphonate)S. *Macromolecules* **2017**, *50*, 7901−7910.

(13) Kwasny, M. T.; Watkins, C. M.; Posey, N. D.; Matta, M. E.; Tew, G. N. Functional Polyethylenes with Precisely Placed Thioethers and Sulfoniums through Thiol−Ene Polymerization. *Macromolecules* **2018**, *51*, 4280−4289.

(14) Reimann, S.; Danke, V.; Beiner, M.; Binder, W. H. Synthesis of Supramolecular Precision Polymers: Crystallization under Conformational Constraints. *J. Polym. Sci. Part A Polym. Chem.* **2017**, *55*, 3736−3748.

(15) Song, S.-F.; Guo, Y.-T.; Wang, R.-Y.; Fu, Z.-S.; Xu, J.-T.; Fan, Z.-Q. Synthesis and Crystallization Behavior of Equisequential ADMET Polyethylene Containing Arylene Ether Defects: Remarkable Effects of Substitution Position and Arylene Size. *Macromolecules* **2016**, *49*, 6001−6011.

(16) Abe, H.; Kikkawa, Y.; Inoue, Y.; Doi, Y. Morphological and Kinetic Analyses of Regime Transition of poly[(S)-Lactide] Crystal Growth. *Biomacromolecules* **2001**, *2*, 1007−1014.

(17) Tsuji, H.; Tezuka, Y.; Saha, S. K.; Suzuki, M.; Itsuno, S. Spherulite Growth of L-Lactide Copolymers: Effects of Tacticity and Comonomers. *Polymer* **2005**, *46*, 4917−4927.

(18) Yasuniwa, M.; Tsubakihara, S.; Iura, K.; Ono, Y.; Dan, Y.; Takahashi, K. Crystallization Behavior of Poly(l-Lactic Acid). *Polymer* **2006**, *47*, 7554−7563.

(19) Zhu, B.; He, Y.; Asakawa, N.; Yoshie, N.; Nishida, H.; Inoue, Y. Polymorphic Crystallization and Melting-Recrystallization Behavior of poly(3-Hydroxypropionate). *Macromolecules* **2005**, *38*, 6455−6465.

(20) Liu, J.; Ye, H.-M.; Xu, J.; Guo, B.-H. Formation of Ring-Banded Spherulites of α and β Modifications in Poly(butylene Adipate). *Polymer* **2011**, *52*, 4619−4630.

(21) Baeten, D. *Fast Scanning Chip Calorimetry Combined with Time Resolved X-Ray Diffraction : A New View on Polymer Crystallization and Melting*; Ph.D. Dissertation, The Katholieke Universiteit Leuven, Flanders, Belgium, 2016.

(22) Blundell, D. J.; Liggat, J. J.; Flory, A. The Crystal Lamellar Morphology of an Aromatic Polyketone with Unusual Crystallization and Melting Behaviour. *Polymer* **1992**, *33*, 2475−2482.

(23) De Rudder, J.; Bergé, B.; Berghmans, H. Competition between Gelation and Crystallization in Solutions of Syndiotactic Polystyrene in Cis-Decalin. *Macromol. Chem. Phys.* **2002**, *203*, 2083−2088.

(24) Cavallo, D.; Zhang, L.; Portale, G.; Alfonso, G. C.; Janani, H.; Alamo, R. G. Unusual Crystallization Behavior of Isotactic Polypropylene and propene/1-Alkene Copolymers at Large Undercoolings. *Polymer* **2014**, *55*, 3234−3241.

(25) Alamo, R. G.; Ghosal, A.; Chatterjee, J.; Thompson, K. L. Linear Growth Rates of Random Propylene Ethylene Copolymers. The Changeover from γ Dominated Growth to Mixed (α+γ) Polymorphic Growth. *Polymer* **2005**, *46*, 8774−8789.

(26) Mollova, A.; Androsch, R.; Mileva, D.; Schick, C.; Benhamida, A. Effect of Supercooling on Crystallization of Polyamide 11. *Macromolecules* **2013**, *46*, 828−835.

(27) Rhoades, A. M.; Williams, J. L.; Androsch, R. Crystallization Kinetics of Polyamide 66 at Processing-Relevant Cooling Conditions and High Supercooling. *Thermochim. Acta* **2015**, *603*, 103−109.

(28) De Santis, F.; Adamovsky, S.; Titomanlio, G.; Schick, C. Isothermal Nanocalorimetry of Isotactic Polypropylene. *Macromolecules* **2007**, *40*, 9026−9031.

(29) Ungar, G.; Keller, A. Inversion of the Temperature Dependence of Crystallization Rates due to Onset of Chain Folding. *Polymer* **1987**, *28*, 1899−1907.

(30) Organ, S. J.; Ungar, G.; Keller, A. Rate Minimum in Solution Crystallization of Long Paraffins. *Macromolecules* **1989**, *22*, 1995−2000.

(31) Higgs, P. G.; Ungar, G. The Growth of Polymer Crystals at the Transition from Extended Chains to Folded Chains. *J. Chem. Phys.* **1994**, *100*, 640−648.

(32) Ungar, G.; Putra, E. G. R.; de Silva, D. S. M.; Shcherbina, M. A.; Waddon, A. J. The Effect of Self-Poisoning on Crystal Morphology and Growth Rates. *Adv. Polym. Sci.* **2005**, *180*, 45−87.

(33) Organ, S. J.; Keller, A.; Hikosaka, M.; Ungar, G. Growth and Nucleation Rate Minima in Long N-Alkanes. *Polymer* **1996**, *37*, 2517−2524.

(34) Chikkali, S.; Stempfle, F.; Mecking, S. Long-Chain Polyacetals from Plant Oils. *Macromol. Rapid Commun.* **2012**, *33*, 1126−1129.

(35) Ortmann, P.; Heckler, I.; Mecking, S. Physical Properties and Hydrolytic Degradability of Polyethylene-like Polyacetals and Polycarbonates. *Green Chem.* **2014**, *16*, 1816.

(36) Kaner, P.; Ruiz-Orta, C.; Boz, E.; Wagener, K. B.; Tasaki, M.; Tashiro, K.; Alamo, R. G. Kinetic Control of Chlorine Packing in Crystals of a Precisely Substituted Polyethylene Toward Advanced Polyolefin Materials. *Macromolecules* **2014**, *47*, 236−245.

(37) Zhang, X.; Santonja-Blasco, L.; Wagener, K. B.; Boz, E.; Tasaki, M.; Tashiro, K.; Alamo, R. G. Infrared Spectroscopy and X-Ray Diffraction Characterization of Dimorphic Crystalline Structures of Polyethylenes with Halogens Placed at Equal Distance along the Backbone. *J. Phys. Chem. B* **2017**, *121*, 10166−10179.

https://dx.doi.org/10.1021/acs.macromol.0c01443
Macromolecules 2020, 53, 7899−7913

(38) Santonja-Blasco, L.; Zhang, X.; Alamo, R. G. Crystallization of Precision Ethylene Copolymers. *Adv. Polym. Sci.* **2017**, *276*, 133−182.
(39) Fraschini, C.; Jiménez, L.; Kalala, B.; Prud'homme, R. E. Polymorphism and Cross-nucleation in Poly 1,3 Dioxolan. *Polymer* **2012**, *53*, 188−195.
(40) Marubayashi, H.; Ushio, T.; Nojima, S. Crystal Polymorphism of Biobased Polyester Composed of Isomannide and Succinic Acid. *Macromolecules* **2019**, *52*, 4624−4633.
(41) Righetti, M. C.; Marchese, P.; Vannini, M.; Celli, A.; Lorenzetti, C.; Cavallo, D.; Ocando, C.; Müller, A. J.; Androsch, R. Polymorphism and Multiple Melting Behavior of Bio-Based Poly(propylene 2,5-furandicarboxylate). *Biomacromolecules* **2020**, *21*, 2622−2634.
(42) Gan, Z.; Kuwabara, K.; Abe, H.; Iwata, T.; Doi, Y. Metastability and Transformation of Polymorphic Crystals in Biodegradable Poly(butylene adipate). *Biomacromolecules* **2004**, *5*, 371−378.
(43) Putra, E. G. R.; Ungar, G. In Situ Solution Crystallization Study of N-$C_{246}H_{494}$: Self-Poisoning and Morphology of Polymethylene Crystals. *Macromolecules* **2003**, *36*, 5214−5225.
(44) Lauritzen, J. I., Jr.; Hoffman, J. D. Extension of theory of growth of chain-folded polymer crystals to large undercoolings. *J. Appl. Phys.* **1973**, *44*, 4340−4352.
(45) Hoffman, J. D.; Davis, G. T.; Lauritzen, J. I., Jr. The Rate of Crystallization of Linear Polymers with Chain Folding. In *Treatise on Solid State Chemistry*; Hannay, N. B., Ed.; Plenum Press: New York, 1976; Vol 3, Chapter 7, pp. 497−614.
(46) Vogel, H. Das Temperaturabhängigkeitsgesetz der Viskosität von Flüssigkeiten. *Phys. Z.* **1921**, *22*, 645−646.
(47) Fulcher, S. G. Analysis of Recent Measurements of the Viscosity of Glasses. *J. Am. Ceram. Soc.* **1925**, *8*, 339−355.
(48) Tamman, V. G.; Hesse, W. Die Abhängigkeit der Viscosität von der Temperatur bie unterkühlten Flüssigkeiten. *Z. Anorg. Allg. Chem.* **1926**, *156*, 245−257.
(49) Hoffman, J. D.; Weeks, J. J. Melting Process and the Equilibrium Melting Temperature of Polychlorotrifluoroethylene. *J. Res. Natl. Bur. Stand., Sect. A* **1962**, *66A*, 13−28.

https://dx.doi.org/10.1021/acs.macromol.0c01443
Macromolecules 2020, 53, 7899−7913